The effect of hydrogen addition on methane/air explosion characteristics in a 20-L spherical device

Baiwei Lei [a,b,*], Qinan Wei [a], Renhua Pang [a], Jianjun Xiao [b,*], Mike Kuznetsov [b], Thomas Jordan [b]

[a] School of Emergency Management and Safety Engineering, China University of Mining & Technology (Beijing), Beijing 100083, China
[b] Institute of Thermal Technologies and Safety, Karlsruhe Institute of Technology, Eggenstein-Leopoldshafen 76344, Germany

ARTICLE INFO

Keywords:
Hydrogen addition
Methane
Maximum deflagration pressure
Heat loss
GASFLOW-MPI

ABSTRACT

The addition of hydrogen to methane changes its deflagration characteristics and increases the combustion rate. However, studies on the effect of hydrogen on methane deflagration remain insufficient. Therefore, based on the CFD code GASFLOW-MPI, a four-step combustion-mechanism model was established for methane/hydrogen mixtures. The deflagration characteristics of a premixed combustible gas in a 20-L spherical device was numerically simulated using a methane/hydrogen/air equivalence ratio of 1 and hydrogen addition in the range of 0–50%; subsequently. The results were compared with experimental data. The four-step methane/hydrogen combustion-mechanism could effectively reproduce the methane/hydrogen deflagration process on considering the heat losses. With an increase in hydrogen addition, the laminar burning velocity increases, and the deflagration duration reduces. It decreases the explosion heat loss and increased the maximum deflagration pressure. Under adiabatic simulation, the maximum deflagration pressure decreased with an increase in hydrogen addition, in contrast with the experimental results. This indicates that the heat-loss effect of the methane/hydrogen/air-mixture deflagration process should not be ignored. Moreover, the heat loss during the methane/hydrogen/air-mixture deflagration was mainly caused by thermal radiation. Thus, the influence of the thermal-radiation and convective heat-transfer mechanisms should be considered in the numerical simulations of methane/hydrogen/air-mixture deflagration.

1. Introduction

With global warming, the development of a low-carbon green economy has become increasingly important in recent years. Studies in the field of energy transformation indicate that the addition of hydrogen to methane increases the combustion rate of fuel, making broad an application perspectives methane/hydrogen mixed fuels energy sources [1–4]. However, hydrogen addition increases the explosion sensitivity of methane, expands the explosion range, and increases the risk of mixed-fuel explosions [5,6]. Therefore, to ensure the safe use of methane/hydrogen mixed fuels, it is necessary to fully understand their deflagration characteristics and the effect of hydrogen addition on the deflagration process.

Numerous studies have analyzed the explosion characteristics of methane/hydrogen/air mixtures [7,8]. The severity of methane/hydrogen fuel explosions can be estimated using several explosion characteristics, such as, the peak pressure, maximum rate of pressure rise, and laminar burning velocity [9]. Experimental analyses indicate that the methane/hydrogen-mixture explosion pressure increase with increasing hydrogen addition [10,11]. For a specific volume ratio of the methane/hydrogen mixture, an increase in the initial pressure increases the explosion peak pressure and maximum pressure rise rate [12–14]. As the initial temperature increases, the explosion peak pressure of the methane/hydrogen mixture decreases, the maximum pressure rise rate increases, and the explosion duration decreases [15]. Moreover, the explosion-characteristic parameters of methane/hydrogen mixtures under different turbulence-intensity conditions have been analyzed [16,17]. Additionally, the effect of hydrogen addition on methane has been investigated in terms of the laminar burning velocity [18–22]. On increasing the hydrogen mole fraction in the fuel, the laminar burning velocity increases linearly up. Di et al. [23] have used the CHEMKIN PREMIX program to calculate the laminar burning velocity of a premixed flame with changing the equivalence ratio (from poor to rich) and fuel composition (from pure methane to pure hydrogen). According to Shen et al. [24], the change in the laminar flame velocity of a methane/hydrogen mixture is mainly affected by the total equivalence ratio.

* Corresponding authors.
E-mail addresses: leibws@cumtb.edu.cn (B. Lei), jianjun.xiao@kit.edu (J. Xiao).

Additionally, studies have confirmed the feasibility of the laminar flame velocity calculation model developed by Dahoe [25,26].

Owing to the transient nature of the deflagration process and the monitoring-method limitations, it is difficult to experimentally monitor the explosion-parameter changes during the explosion process. Numerical simulations are more suitable for a detailed analysis of the key explosion parameters, to understand the mechanism of flame propagation and pressure rise [27–29]. Adiabatic simulations of methane/hydrogen explosions indicate that the explosion peak pressure decreases on increasing hydrogen addition [30,31]; this is contrary to the experimental results, and could be due to heat loss [15,32]. However, there are very few quantitative studies on the effect of hydrogen addition on the explosion-related heat loss. Leyer et al. [33] have evaluated the heat loss during an explosion in a closed container by evaluating the difference between the theoretical internal energy of the combustion gas and experimental data. Numerous studies have used this method to calculate the heat loss during explosion [34,35]; however, this method is unable calculate the contribution of various heat-transfer mechanisms to the total heat loss. Zhang et al. [36] have considered methane/hydrogen mixture combustion reactions to be rapid processes and included only the surface heat transfer in the explosion heat-loss (neglecting the volumetric radiative heat loss). However, according to Goldfarb et al. [37], the effect of thermal radiation on combustible-gas explosions is significant and cannot be ignored. The numerical simulation results on a methane/air explosion by Lei et al. [38] also indicate that thermal radiation is the most important factor causing heat loss during a methane explosion. A review of the aforementioned literature indicated that the numerical simulation of heat losses in the explosion process of methane/hydrogen premixed gases require further investigation. The adiabatic-simulation method does not reflect the actual explosion process, and the accuracy of the simulation results requires analysis and improvement.

Considering the lack of the methane/hydrogen/air-mixture explosion experiment and numerical simulations, this study develops an explosion model with a four-step methane/hydrogen combustion mechanism using the GASFLOW-MPI code. Additionally, a mathematical model of the heat-transfer mechanism was incorporated into the model to calculate the ratio of convective heat transfer and thermal radiation in the total heat loss during a methane/hydrogen-mixture explosion.

2. Mathematical modeling

GASFLOW-MPI is an all-speed CFD code with parallel scalability that uses a robust implicit continuous Eulerian–arbitrary Lagrangian-Eulerian solution algorithm (ICE'd-ALE) to solve compressible Navier-Stokes equations [39]. This section briefly introduces the governing equations, heat-transfer model, and reaction mechanism.

2.1. Governing equations

(1) Mass conservation equation:

The mass conservation equation of a methane/hydrogen mixed gas is [40]:

$$\frac{d}{dt}\int_V \rho dV = \oint_S \rho u dS + \int_V S_{\rho,com} dV \tag{1}$$

where V denotes the fluid control volume, S denotes the control surface, u denotes the mass average velocity vector, and $S_{\rho,com}$ denotes the mass source term.

The transport equation for each gas specie is:

$$\frac{d}{dt}\int_V \rho_\alpha dV = \oint_S [\quad \rho_\alpha u + J_\alpha] dS + \int_V S_{\rho,\alpha,com} dV \tag{2}$$

where α is the gas specie,ρ_α denotes the macroscopic density, which indicates the mass of each specie per unit volume, J_α is the diffusion term of the specieα, and $S_{\rho,\alpha,com}$ represents the change in the mass of the specie due to hydrogen combustion in the case considered. The specific formula for the J_α parameter can be found in the literature [40,41].

(2) Momentum-conservation equation:

The momentum conservation equation is [38,40]:

$$\frac{d}{dt}\int_V \rho u dV = \oint_S [\quad \rho u u \quad P \quad \tau] dS + \int_V \rho g dV \tag{3}$$

where P denotes the pressure, τ denotes the viscous stress tensor, and g denotes the gravitational vector.

(3) Energy conservation equation

The energy conservation equation is [38,40]:

$$\frac{d}{dt}\int_V \rho I dV = \oint_S [\quad \rho I u \quad P u \quad q] dS + \int_V \left(S_{I,com} + S_{I,conv} + S_{I,rad} + S_{I,cond}\right) dV \tag{4}$$

where $S_{I,com}$ is the energy source term owing to combustion. The heat-transfer mechanisms, such as convection, radiation, and steam condensation, were calculated using $S_{I,conv}$, $S_{I,rad}$, and $S_{I,rad}$, respectively.

2.2. Turbulence model

Detached-Eddy Simulation (DES) turbulence model is used in this study. DES turbulence model is a hybrid turbulence model of Large-Eddy Simulation (LES) and Reynolds-Averaged Navier-Stokes (RANS), which has been successfully applied in numerous industrial applications [55].

2.3. Heat transfer models

(1) Convective heat-transfer model:

The convective heat transfer between the gas and explosive spherical device can be represented by the following [42]:

$$S_{I,conv} = h_s A_s (T_s \quad T) \tag{5}$$

where h_s is the surface heat transfer coefficient, A_s is the exposed area of the inner wall of the calculation unit, T_s is the surface temperature of the spherical device, and T is the gas temperature.

By simplifying the Reynolds analogy formula and combining it with the Chilton-Colburn empirical analogy between the momentum and thermal boundary layers, the heat transfer coefficient h_s can be obtained by the following equation [42,43]:

$$h_s = \frac{\tau_s}{|u_c|} C_p \cdot Pr^{-\frac{2}{3}} \tag{6}$$

where τ_s is the wall shear stress, u_c is the average speed of the unit center, C_p is the specific heat capacity, and Pr is the Prandtl number.

(2) Thermal radiation model:

Thermal radiation plays an important role in methane/hydrogen deflagration. Methane/hydrogen/air-mixture deflagration involve gas mixtures, including CH_4, H_2, N_2, O_2, CO, CO_2, and H_2O [44,47]. Most of the flame radiation during deflagration is caused by water vapor and CO_2 (the radiation of the other gas components is negligible compared to that of water vapor and CO_2); therefore, only the H_2O absorption data can be determined [45–47]. Assuming the gas to maintain thermodynamic equilibrium locally, the transport equation of the gray gas thermal radiation can be represented by the following [47–49]:

$$\frac{1}{c}\frac{\partial E(r,\Omega,t)}{\partial t}+l_i\frac{\partial E(r,\Omega,t)}{\partial x_i}= \quad \alpha E(r,\Omega,t)+\frac{\alpha\sigma T^4}{\pi} \tag{7}$$

where c is the speed of light, α is the absorption coefficient, σ is the Stefan-Boltzmann constant, and T is the gas temperature. $E(r,\Omega,t)$ is a function of the position vector$r$, direction vectorΩ, and time$t$. In addition, l_i is the direction cosine of the vector Ω relative to the coordinate directionx_i.

The differential approximation method can be used to approximate equation (7). The approximate differential equation of the radiation energy density,U^r, and radiation flux vector,l_i, is given by the following [47]:

$$\frac{\partial U^r}{\partial t}+\frac{\partial q_i}{\partial x_i}=\frac{c}{\lambda}(\partial T^4 \quad U^r) \tag{8}$$

$$q_i= \quad \frac{c\lambda}{3}\frac{\partial U^r}{\partial x_i} \tag{9}$$

2.4. Reaction mechanism

Numerous studies indicate that the volatile gas components produced during biomass conversion include CO, CO_2, CH_4, and H_2 [50,51]. The Jones' four-step global mechanism can be used to understand the combustion of mixed gases [52,53]. It is represented by the following equations:

$$CH_4+0.5O_2\rightarrow CO+2H_2 \tag{10}$$

$$CH_4+H_2O\rightarrow CO+3H_2 \tag{11}$$

$$CO+H_2O\leftrightarrow CO_2+H_2 \tag{12}$$

$$H_2+0.5O_2\leftrightarrow H_2O \tag{13}$$

Equations (10) and (11), describing the reaction of methane, are dominant in lean and rich fuel mixtures, respectively [54]. Equation (12) describes the conversion of CO to H_2O, while equation (13) describes the oxidation of hydrogen. To reduce the computational time for chemical-equilibrium calculations in this global mechanism, all the reactions are considered to be irreversible [53].

The forward reaction rates for four reactions can be written as:

$$\dot{\omega}_{f,1}=C_{f,1}T^{n1}e^{\left(-E_{a,1}/RT\right)}[CH_4]^{0.5}[O_2]^{1.25} \tag{14}$$

$$\dot{\omega}_{f,2}=C_{f,2}T^{n2}e^{\left(-E_{a,2}/RT\right)}[CH_4]^{1}[H_2O]^{1} \tag{15}$$

$$\dot{\omega}_{f,3}=C_{f,3}T^{n3}e^{\left(-E_{a,3}/RT\right)}[CO]^{1}[H_2O]^{1} \tag{16}$$

$$\dot{\omega}_{f,4}=C_{f,4}T^{n4}e^{\left(-E_{a,4}/RT\right)}[H_2]^{0.25}[O_2]^{1.5} \tag{17}$$

where C_f is the frequency factor, n is the temperature exponent, E_a is the activation energy. The subscripts 1, 2, 3, and 4 respectively denote the four reactions. The reaction parameters are summarized in Ref. [52].

3. GASFLOW-MPI modelling

3.1. Experimental layout

The explosion experiment of a methane/hydrogen mixture in a 20-L spherical device conducted by Ma et al. [31] was selected for simulation in this study. Fig. 1 shows the geometric model of the 20-L spherical device. The experimental apparatus consisted of an explosion vessel, electric ignition system, and data acquisition system. The ignition source was located in the center of the 20-L spherical device, and the pressure and temperature monitoring points were located on the inner walls of the explosion vessel. In the experiment, 99.99 % pure methane and hydrogen were used. All the additional experimental details are mentioned in Ref. [31].

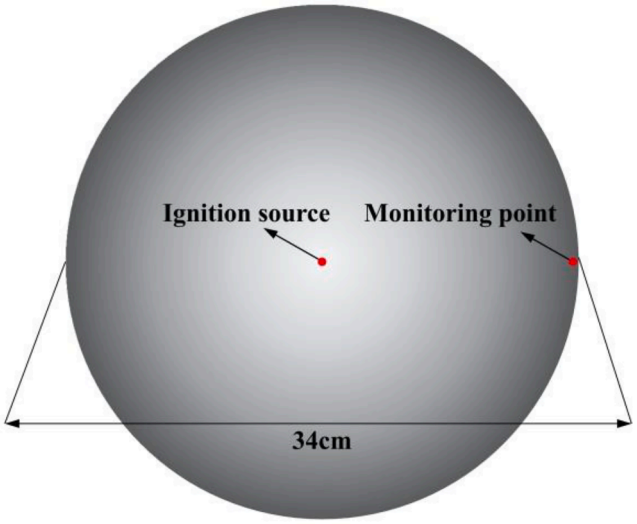

Fig. 1. Geometric model of the 20-L explosion-reaction vessel.

3.2. Numerical simulation set-up

The following hydrogen addition (volume fraction of hydrogen) was used in the numerical simulation:

$$X_{H_2}=\frac{V_{H_2}}{V_{H_2}+V_{CH_4}} \tag{18}$$

where X_{H_2} is the hydrogen addition, V_{H_2} is the hydrogen volume, and V_{CH_4} is the methane volume.

The following fuel equivalence ratio was used in the numerical simulation:

$$\phi=\frac{(F/A)}{(F/A)_{stoic}} \tag{19}$$

where ϕ is the fuel equivalent ratio, (F/A) is the fuel–air ratio, and $(F/A)_{stoic}$ is the stoichiometric ratio of fuel to air.

Here, three-dimensional modeling was conducted according to the geometric size of the 20-L spherical device described in Ref. [31]. The initial ambient temperature and atmospheric pressure of the spherical device were 300 K and 0.1 MPa, respectively. Four premixed gases with equivalence ratios of 1 and methane/hydrogen volume ratios from 100:0 to 50:50 were prepared, as listed in Table 1. The gravitational acceleration was set to 9.8 m/s^2. The wall material of the spherical explosive device is steel, the density (ρ) is 7850 kg/m^3, the specific heat at constant pressure (C_p) is 490 J/kg·K, the heat transfer coefficient (K) is 50 W/m·K, and the emissivity coefficient is 0.85.

For high calculation accuracy and computational efficiency, the computational domain was set as a uniform grid with a 3D-mesh size of 6.6 mm (L) × 6.6 mm (W) × 6.6 mm (H). The number of grids set in the x-, y-, and z-axes directions was 53, with a total of 148,877 grids. The

Table 1
Mixture compositions in the numerical simulations conducted at 300 K and 0.1 MPa.

X_{H_2}	$\Phi=1$		
	Hydrogen/%	Methane/%	Air/%
0 %	0	9.5	90.5
10 %	1.02	9.17	89.81
30 %	3.58	8.35	88.07
50 %	7.19	7.19	85.62

geometric model of the 20-L spherical device was divided into two different types of grid numbers to verify the reasonability of the number of grids and their independence in the numerical simulation. Fig. 2 shows the pressure-change curves in the spherical device with 148,877 and 297,754 grids. The simulation results for the two types of mesh numbers were the same. Therefore, to improve the computational efficiency, 148,877 numerical simulation model grids were used in this study.

4. Results and discussion

4.1. Accuracy verification of the simulation results

In this study, adiabatic and heat-loss simulations (simulations considering heat loss) were used to quantitatively analyze the effect of hydrogen addition on the methane deflagration characteristics. Fig. 3 compares the experimental and simulation results of the maximum deflagration pressures with different hydrogen additions at an equivalent ratio (Φ) of 1. A linear relationship was observed between the maximum deflagration pressure and hydrogen addition. In the adiabatic simulation, the maximum deflagration pressure decreased with increasing hydrogen addition. The simulation results were not in agreement with the experimental results. Contrarily, in the heat-loss simulation, the maximum deflagration pressure was consistent with the experimental results. Therefore, calculating the heat loss is crucial for studying the deflagration process. Fig. 4 compares the experimental and simulation results of the maximum pressure rise rates of the deflagration with different hydrogen additions at $\Phi = 1$. The adiabatic and heat-loss simulation results were consistent with the experimental results, with the latter exhibiting a slightly better agreement. Therefore, the numerical model considering heat loss accurately reflected the actual methane/hydrogen/air-mixture deflagration process.

4.2. Pressure

Fig. 5 shows the adiabatic simulation results of the deflagration pressure–time for different hydrogen additions. Fig. 6 shows the simulation results of the deflagration pressure–time with different hydrogen additions considering heat loss. Both the simulation results showed the same trend before the deflagration pressure reached the peak value; subsequently, when the deflagration pressure reached the peak value, the adiabatic simulation ignored the heat loss during deflagration, and the deflagration pressure remained constant at the peak value. Contrarily, in the heat-loss simulation, the deflagration pressure decayed after reaching the peak value, because the high-temperature gas

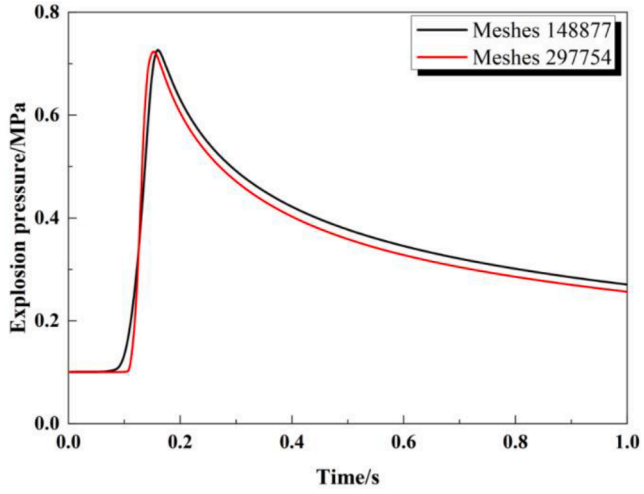

Fig. 2. Mesh sensitivity analysis.

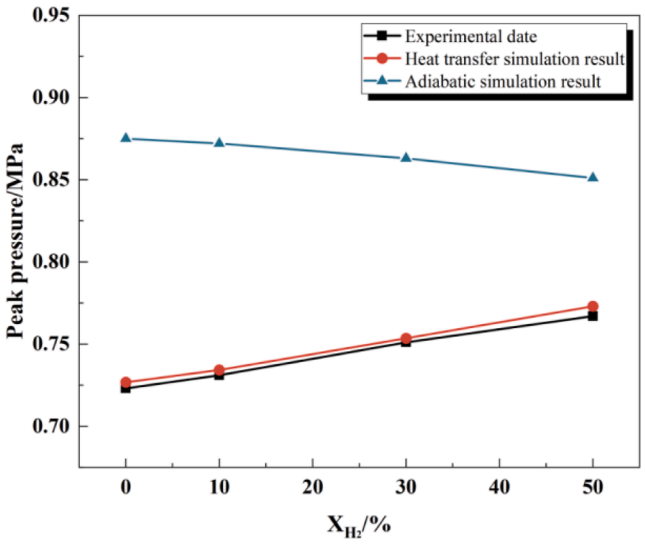

Fig. 3. Comparison of the measured and calculated peak pressures of deflagration.

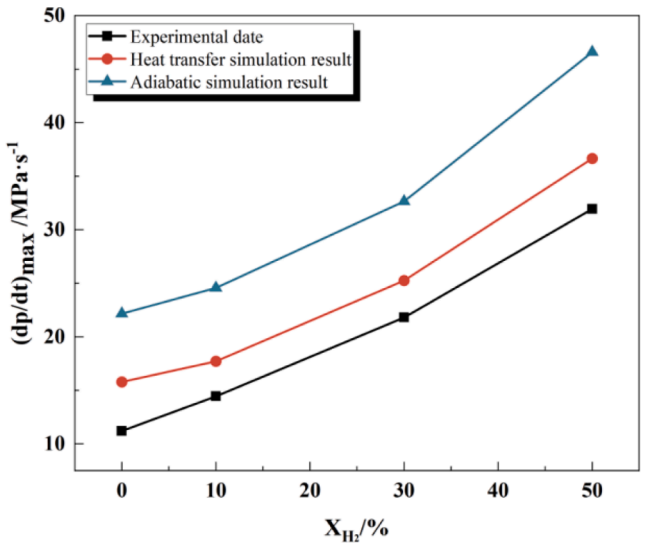

Fig. 4. Comparison of the measured and calculated maximum pressure rise rates of deflagration.

product generated by the reaction continued to transfer heat to the side wall.

The term t_e indicates the duration of a methane/hydrogen/air-mixture deflagration [15]. According to Fig. 6, compared to a pure methane explosion with 0 % hydrogen addition, the deflagration duration decreased (by 8.7 %, 32.2 %, and 50.3 %) on adding 10 %, 30 %, and 50 % hydrogen. The addition of hydrogen possibly increased the chemical reaction rate of methane due to its rapid reactivity, shortening the deflagration duration.

As mentioned in Section 4.1, the adiabatic and heat-loss simulation results of the maximum deflagration pressure showed opposite trends with hydrogen addition. Under adiabatic simulation, compared to a pure methane deflagration with 0 % hydrogen addition, the maximum deflagration pressure decreased by 0.6 %, 1.3 %, and 2.9 % on increasing the hydrogen addition. This phenomenon could be attributed to the significantly lower heating value (LHV) of hydrogen compared to that of methane [30]. In the adiabatic simulation without heat loss, a lower total heat was released by the reaction on adding more hydrogen to the spherical device, decreasing the maximum deflagration pressure.

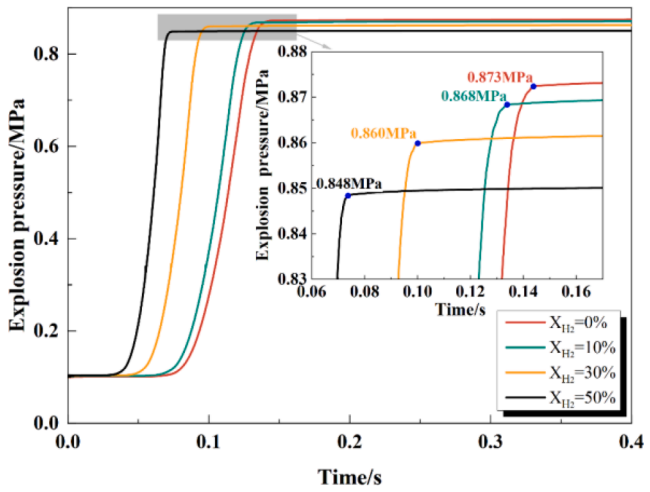

Fig. 5. Adiabatic simulations of the methane/hydrogen-mixture deflagration pressure curves.

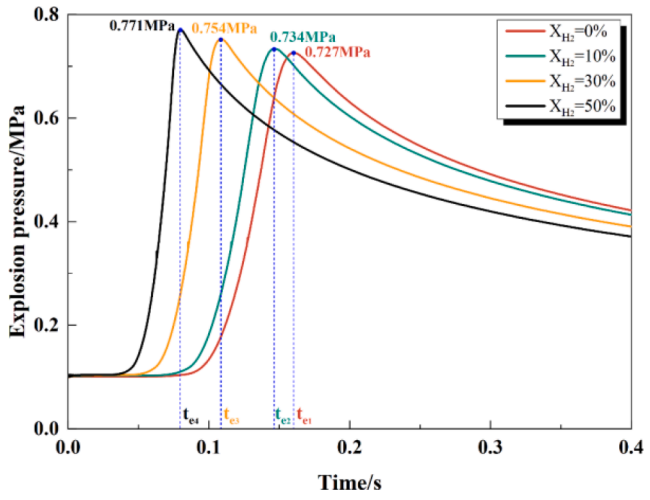

Fig. 6. Heat-loss simulations of the methane/hydrogen-mixture deflagration pressure curves.

However, the simulation results considering the effect of heat loss on the deflagration process were different. With increasing hydrogen addition, the maximum deflagration pressure increased by 0.9 %, 3.7 %, and 6.0 %. Hydrogen can accelerate the chemical reaction rate of methane and accelerate the heat release rate of the mixture. However, hydrogen addition also shortens the deflagration duration. The sudden rise of temperature in the spherical explosive device will lead to the acceleration of radiation heat transfer rate, but the fast reactivity of hydrogen shortens the heat-transfer time, which leads to a decrease in total heat loss. Therefore, the maximum deflagration pressure will increase with the increase of hydrogen addition.

4.3. Maximum rate of pressure rise

Fig. 7 shows the simulation results of the deflagration pressure-rise rate with different hydrogen additions, considering heat loss. The maximum rate of pressure rise increased with increasing hydrogen addition. Hydrogen addition shortens the deflagration duration; therefore, the time to reach the peak pressure-rise rate decreased on increasing hydrogen addition.

According to a formula derived by Dahoe [26] for calculating the pressure-rise rate, the maximum pressure-rise rate can be explained by the maximum deflagration pressure and laminar burning velocity, as

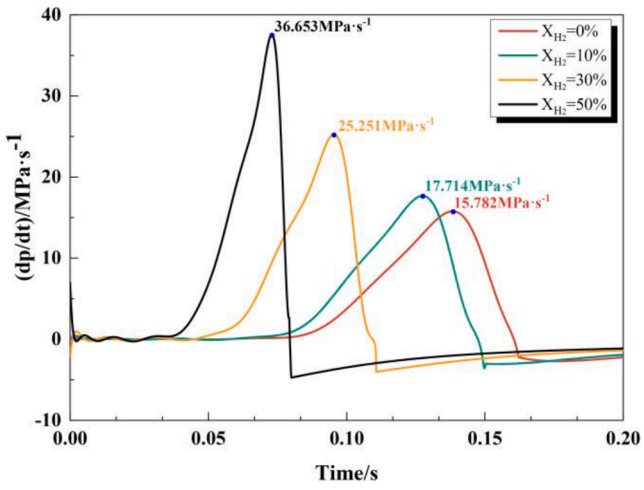

Fig. 7. Heat-loss simulations of the methane/hydrogen-mixture deflagration pressure-rise-rate curves.

follows:

$$\frac{dP}{dt} = 3(P_{\max} \quad P_0)\left(\frac{4\pi}{3V_V}\right)^{1/3}\left[1 \quad \left(\frac{P_0}{P}\right)^{1/\gamma}\frac{P_{\max}}{P_{\max}} \quad \frac{P}{P_0}\right]^{2/3}\left(\frac{P}{P_0}\right)^{1/\gamma} S_{uL} \tag{20}$$

where $P_{\max}$ is the deflagration peak pressure, P_0 is the initial pressure, P is the deflagration pressure, V_V is the explosion vessel volume, S_{uL} is the laminar burning velocity, and γ is the adiabatic coefficient of the unburnt mixture.

The laminar burning velocity increases 1.5–2 times with hydrogen addition to 50 % [18–22]. The maximum deflagration pressure is also increases due to less heat losses (Fig. 6). Then, these two factors leading to the maximum pressure-rise rate to increase with the increase of hydrogen concentration.

4.4. Velocity and temperature of the gas

Fig. 8 (a) shows the airflow velocity field when the pressure reaches the peak with different hydrogen additions. As shown in Fig. 8 (a), the gas in the spherical explosive device diffused outward under the action of the pressure wave, while it showed a bottom-up movement due to buoyancy. The outer airflow was compressed and moved to the center of the spherical device after hitting the side wall. At this time, the maximum airflow velocity increased with increasing hydrogen addition. With adding 0 %, 10 %, 30 %, and 50 % hydrogen, the maximum airflow velocities of 4.89 m/s, 5.30 m/s, 5.75 m/s, and 9.65 m/s, respectively, were observed. The outward-diffused gas was compressed and moved toward the center of the spherical device, and the velocity difference between the outward-diffusing gas and inward-moving gas generated a vortex in the flow field. Fig. 8 (b) shows the airflow velocity field at 0.4 s with different hydrogen additions. Subsequently, on completion of the combustion reaction, the explosion pressure wave gradually disappeared, and the gas in the spherical explosion device mainly moved from bottom to top under buoyancy. Therefore, at 0.4 s, the airflow velocity in the middle of the spherical device decreased with increasing hydrogen addition. The gas was compressed on hitting the upper wall of the sphere, and it rebounded, forming a vortex ring near the side walls of the spherical device.

Fig. 9 shows the gas-mass and temperature change curves generated by the heat-loss simulation. The explosion peak-temperature increased with increasing hydrogen addition. Peak temperatures of 2179 K, 2212 K, 2299 K, and 2397 K, were observed for hydrogen additions from 0 % to 50 %. According to the gas-mass change curve, during the deflagration process, as the amount of hydrogen added increased, the mass consumption rate of CH_4 and mass generation rates of CO and CO_2

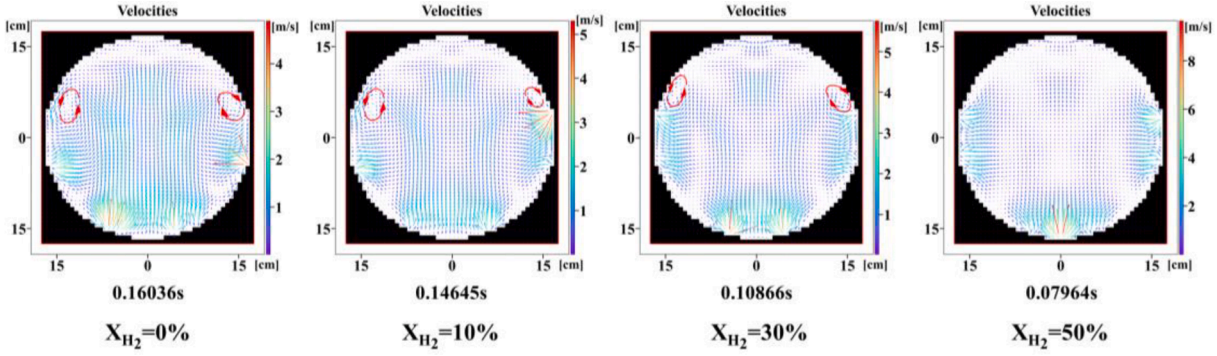

a. The airflow velocity field when the deflagration pressure reaches the peak value.

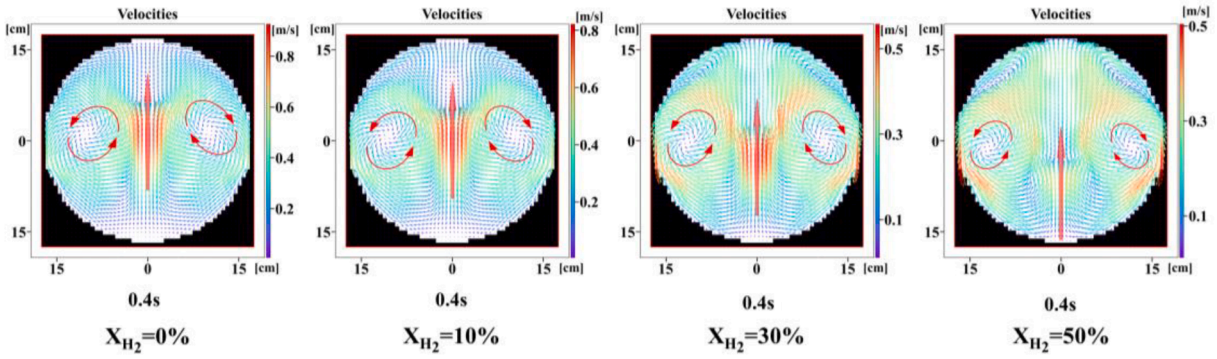

b. The airflow velocity field at 0.4 s.

Fig. 8. Airflow velocity-field distributions.

gradually increased. The gas-mass change rate accelerated after adding hydrogen, confirming the ability of hydrogen to accelerate the chemical reaction rate. Additionally, as indicated by Fig. 9 (a), when the hydrogen addition was 0 %, the hydrogen in the mixed gas was entirely generated by the methane combustion reaction. According to Fig. 9 (b), when the hydrogen addition was 10 %, the hydrogen quality showed an upward trend in the time range of 0.075–0.1 s. According to Fig. 9 (c) and (d), the hydrogen mass did not show an upward trend for 30 % and 50 % hydrogen addition. Thus, when the hydrogen addition exceeded 30 %, the added-hydrogen content was significantly larger than that generated by the methane reaction, and the added hydrogen dominated the reaction.

4.5. Heat loss

Fig. 10 shows the total heat release, heat loss, and heat-loss-rate curves of the deflagration with different hydrogen additions for the heat-loss simulation. Stage I was the combustion reaction stage, with t_e as the critical point (with up to 99.9 % methane/hydrogen consumption). In stage I, a heat-release process started immediately after the methane/hydrogen/air-mixture deflagration. The total heat release of the combustion reaction reached a peak value when the methane/hydrogen completely reacted. At this stage, the high-temperature flame and gas products produced by the deflagration predominated the heat-loss process, and the total heat loss continued to increase. Since the LHV of hydrogen is lower than that of methane, the total heat release decreased with increasing hydrogen addition. In stage II, the combustion reaction ended, and the total heat release of the combustion reaction remained unchanged after reaching the peak value. At this stage, the high-temperature gas products lost heat to the side wall, and the total heat loss continued to increase. The heat accumulated in the spherical device during the deflagration can be calculated by subtracting the lost heat from the total heat released by the combustion reaction [34]:

$$Q_{accumulated} = Q_{released} \quad Q_{transferred} \tag{21}$$

where $Q_{accumulated}$ is the heat accumulated in the spherical device, $Q_{released}$ is the total heat released by the combustion reaction, and $Q_{transferred}$ is the heat transferred by the high-temperature flame and gas products to the side wall (total heat loss). As shown in Fig. 10, the end time of the combustion reaction (t_e) always lagged behind the corresponding time of the maximum heat-loss rate. With an increase in hydrogen addition, the gap between the two gradually decreased.

According to the heat loss curve (Fig. 10), the total heat loss in the deflagration process (stage I) decreased with increasing hydrogen addition. For hydrogen additions of 0 %, 10 %, 30 %, and 50 %, the total heat losses were 10.074 kJ, 9.332 kJ, 7.719 kJ, and 5.633 kJ, respectively. This can be explained using the following equation:

$$Q_{transferred} = \int H_{rate} dt \tag{22}$$

where $Q_{transferred}$ is the total heat loss, H_{rate} is the heat-loss rate, and dt is the heat-loss time during the deflagration. The heat-loss rate characterizes the heat loss per unit time. The total heat loss was proportional to the heat loss rate and time. Compared to a pure methane deflagration with 0 % hydrogen addition, the heat loss rate increased by 4.6 %, 18.6 %, and 37.5 %, respectively, with adding 10 %, 30 %, and 50 % hydrogen, while the heat-loss times were reduced by 8.8 %, 31.9 %, and 50 %, respectively. Therefore, with an increase in hydrogen addition, the decrease in heat-loss time was more significant than the increase in the heat-loss rate. According to equation (18), the total heat loss

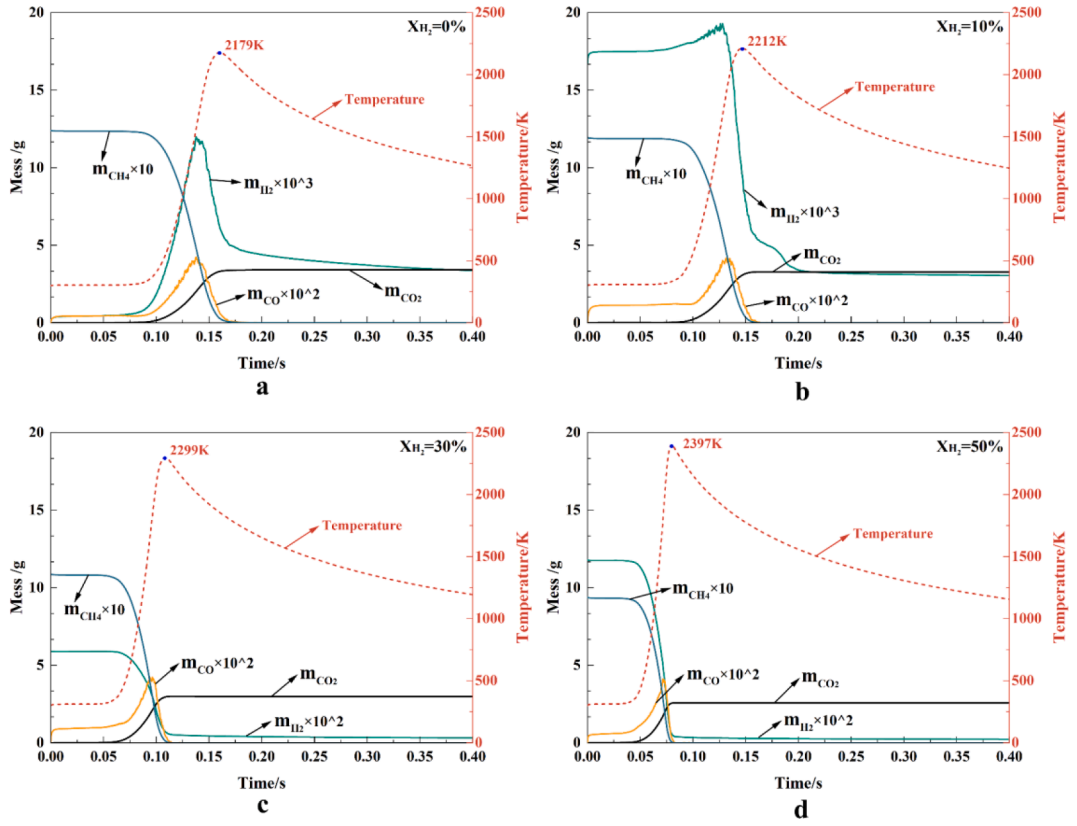

Fig. 9. Explosion gas-mass and temperature curves.

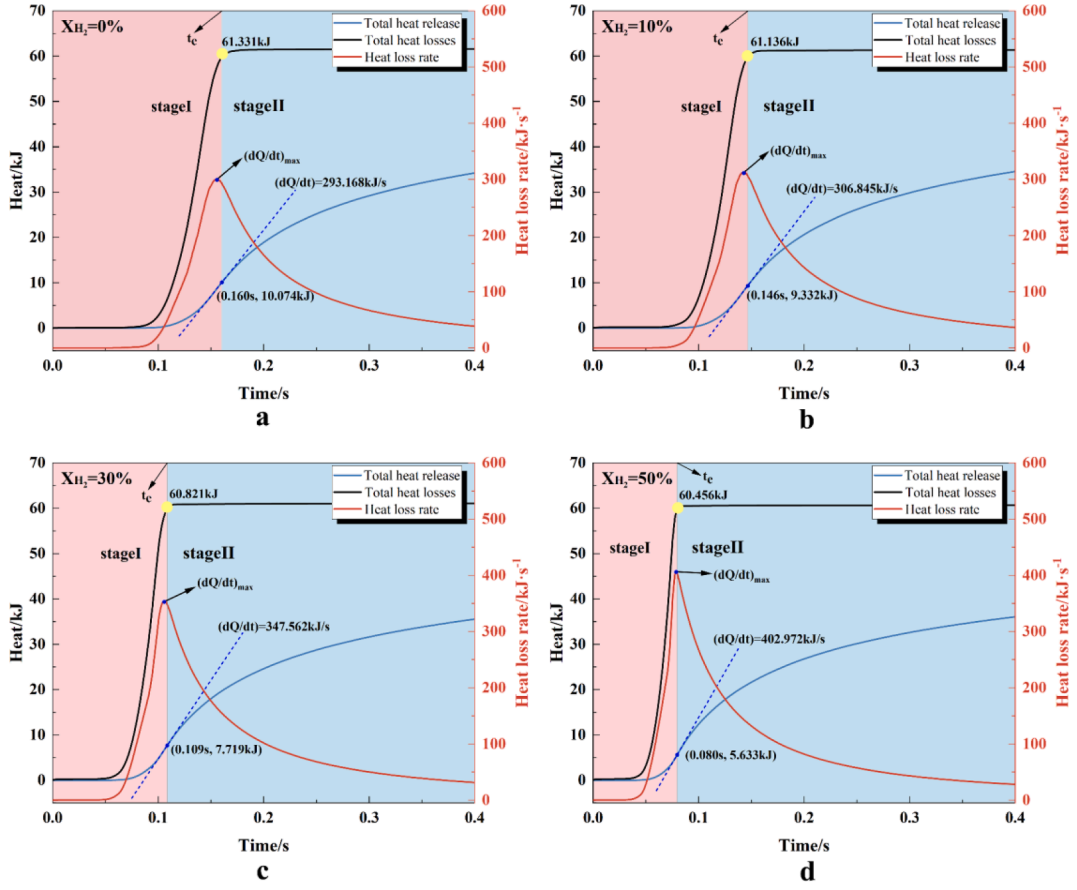

Fig. 10. The total heat release, heat loss, and heat-loss-rate curves of the deflagration.

obtained by multiplying the two values decreased with an increase in hydrogen addition.

Fig. 11 shows the thermal radiation rate and convective heat transfer rate curves. The thermal-radiation start-up time was always less than that of the convective heat-transfer process. This phenomenon could be attributed to the instantaneous production of high-temperature air mass by the rapid induction of the thermal-radiation mechanism by the methane/hydrogen/air-mixture deflagration, and gradual induction of the convective heat transfer efficiency (limited by the flow field speed). Moreover, the heat radiation and convective heat transfer rates increased with increasing hydrogen addition. For a pure methane deflagration with 0 % hydrogen, the peak rates of thermal radiation and convective heat transfer were 221.441 kJ/s and 85.082 kJ/s, respectively; the maximum thermal radiation rate increased by 4.0 %, 17.8 %, and 33.9 %, respectively, for hydrogen additions of 10 %, 30 %, and 50 %, while the maximum convective heat transfer rate increased by 4.8 %, 17.1 %, and 33.9 %, respectively. After adding hydrogen to methane, the fast reactivity of hydrogen shortened the time of explosion significantly, causing a rapid accumulation of heat in the spherical device, a rapid increase in temperature, and an exponential increase of the thermal radiation rate. The increase in the convective heat transfer rate was possibly due to an increase of the temperature difference between the high-temperature gas product and the sphere wall after hydrogen addition.

The green and yellow colored areas in Fig. 11 represent heat lost by the thermal-radiation and convective heat-transfer mechanisms, respectively. In the combustion reaction process (Stage I), when the hydrogen addition was 0 %, 10 %, 30 %, and 50 %, the thermal-radiation mechanism accounted for 84.9 %, 85.8 %, 86.7 %, and 89.1 % of the total heat loss, respectively, while the convective heat-transfer mechanism accounted for 15.1 %, 14.2 %, 13.3 %, and 10.9 % of the total heat loss, respectively. Thus, thermal radiation was the primary heat-loss mechanism in the combustion reaction of methane/hydrogen/air mixtures, and increasing the hydrogen addition increased the proportion of thermal-radiation heat transfer.

5. Conclusion

In this study, a four-step combustion-mechanism model for methane/hydrogen mixtures, based on the CFD code GASFLOW-MPI and the deflagration process of methane/hydrogen/air mixtures, was numerically simulated. To compare the numerical simulation and experimental results, the influence of hydrogen addition into a 20-L spherical device on the deflagration characteristics of methane/hydrogen/air mixtures were analyzed in detail. For the adiabatic simulation, the maximum deflagration pressure decreased with an increase in hydrogen addition. This is inconsistent with the experimental results. However, the simulation results of the maximum deflagration pressure (considering heat-loss) increased on increasing hydrogen addition. This is consistent with the experimental results. Therefore, the heat-loss effect of methane/hydrogen/air-mixture deflagration in the 20-L spherical device should not be ignored. For the simulation considering heat-loss, adding hydrogen to methane accelerated the chemical-reaction and laminar-combustion rates. The higher reactivity of hydrogen caused a shorter deflagration duration (t_e), and the heat-loss time of the high-temperature flame to the ball wall was shortened. Finally, in the heat-loss simulation, the maximum deflagration pressure increased with an increase in hydrogen addition. Thus, the change in

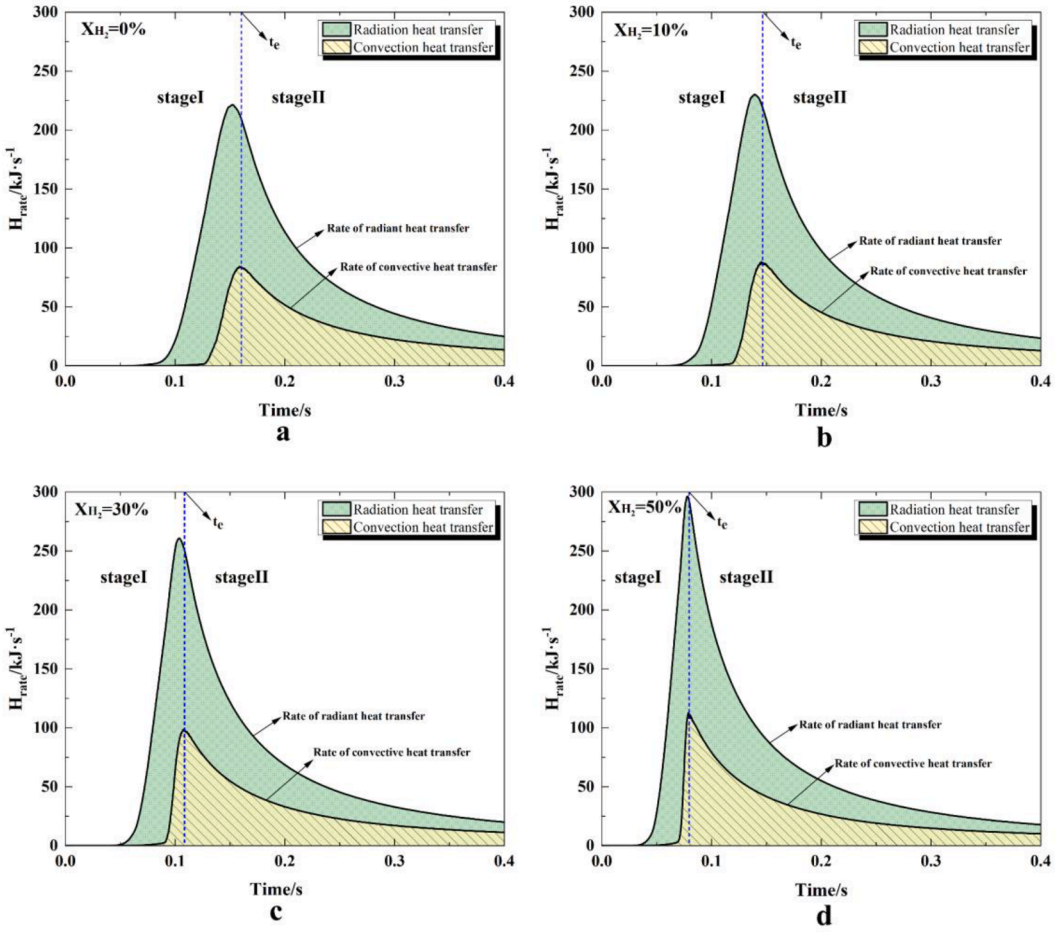

Fig. 11. Rate of change curves of heat radiation and convective heat loss.

heat loss mechanism caused by hydrogen addition during the deflagration of methane/hydrogen/air mixtures was the main reason for the increase in the maximum deflagration pressure. Additionally, thermal radiation was identified to be the dominant heat-loss mechanism during the deflagration of methane/hydrogen/air. For hydrogen additions of 0 %, 10 %, 30 %, and 50 %, the thermal-radiation mechanism accounted for 84.9 %, 85.8 %, 86.7 %, and 89.1 % of the total heat loss, respectively. Therefore, increasing hydrogen addition enhanced the contribution of thermal-radiation heat loss.

CRediT authorship contribution statement

Baiwei Lei: Methodology, Software, Validation, Writing – original draft. **Qinan Wei:** Validation, Writing – original draft. **Renhua Pang:** Writing – review & editing. **Jianjun Xiao:** Writing – review & editing. **Mike Kuznetsov:** Writing – review & editing. **Thomas Jordan:** Writing – review & editing.

Declaration of Competing Interest

The authors declare that they have no known competing financial interests or personal relationships that could have appeared to influence the work reported in this paper.

Data availability

Data will be made available on request.

Acknowledgements

The authors would like to acknowledge the basic scientific research business expenses of Central Universities (grant No. 2022YQAQ09). Baiwei Lei was also like to acknowledge China Scholarship Council for its financially supported.

References

[1] Jones DR, Al-Masry WA, Dunnill CW. Hydrogen-enriched natural gas as a domestic fuel: an analysis based on flash-back and blow-off limits for domestic natural gas appliances within the UK. Sustain Energy Fuels 2018;2(4):710–23.
[2] Mardani A, Mahalegi HKM. Hydrogen enrichment of methane and syngas for MILD combustion. Int J Hydrogen Energy 2019;44(18):9423–37.
[3] Momirlan M, Veziroglu T. The properties of hydrogen as fuel tomorrow in sustainable energy system for a cleaner planet. Int J Hydrogen Energy 2005;30(7):795–802.
[4] Mayrhofer M, Koller M, Seemann P, Prieler R, Hochenauer C. Assessment of natural gas/hydrogen blends as an alternative fuel for industrial heat treatment furnaces. Int J Hydrogen Energy 2021;46(41):21672–86.
[5] Emami SD, Rajabi M, Hassan CRC, Hamid MDA, Kasmani RM, Mazangi M. Experimental study on premixed hydrogen/air and hydrogen–methane/air mixtures explosion in 90 degree bend pipeline. Int J Hydrogen Energy 2013;38(32):14115–20.
[6] Wang L-Q, Ma H-H, Shen Z-W, Chen D-G. The influence of an orifice plate on the explosion characteristics of hydrogen-methane-air mixtures in a closed vessel. Fuel 2019;256:115908.
[7] Zheng K, Yu M, Zheng L, Wen X, Chu T, Wang L. Experimental study on premixed flame propagation of hydrogen/methane/air deflagration in closed ducts. Int J Hydrogen Energy 2016;42(8):5426–38.
[8] Yu M, Zheng K, Zheng L, Cu T, Guo P. Effects of hydrogen addition on propagation characteristics of premixed methane/air flames. J Loss Prev Process Ind 2015;34: 1–9.
[9] Liu L, Luo Z, Wang T, Cheng F, Gao S, Liang H. Effects of initial temperature on the deflagration characteristics and flame propagation behaviors of CH_4 and its blends with C_2H_6, C_2H_4, CO, and H_2. Energy Fuels 2020;35(1):785–95.
[10] Ma Q, Zhang Q, Pang L. Hazard effects of high-speed flow from methane-hydrogen premixed explosions. Process Safe Prog 2014;33(1):85–93.
[11] Huang K, Sun ZY, Tian YC, Wang KL. Turbulent combustion evolution of stoichiometric H_2/CH_4/air mixtures within a spherical space. Int J Hydrogen Energy 2020;45(17):10613–22.
[12] Salzano E, Cammarota F, Di Benedetto A, Sarli VD. Explosion behavior of hydrogen–methane/air mixtures. J Loss Prev Process Ind 2012;25(3):443–7.
[13] Faghih M, Gou X, Chen Z. The explosion characteristics of methane, hydrogen and their mixtures: a computational study. J Loss Prev Process Ind 2016;40:131–8.
[14] Ma Q, Zhang Q, Pang L, Huang Y, Chen J. Effects of hydrogen addition on the confined and vented explosion behavior of methane in air. J Loss Prev Process Ind 2014;27:65–73.
[15] Li R, Luo Z, Wang T, Cheng F, Lin H, Zhu X. effect of initial temperature and H_2 addition on explosion characteristics of H_2-poor/CH_4/air mixtures. Energy 2020;213:118979.
[16] Mandilas C, Ormsby MP, Sheppard C, Woolley R. Effects of hydrogen addition on laminar and turbulent premixed methane and iso-octane–air flames. Proc Combust Inst 2007;31(1):1443–50.
[17] Sun ZY. Experimental studies on the explosion indices in turbulent stoichiometric H_2/CH_4/air mixtures. Int J Hydrogen Energy 2019;44(1):469–76.
[18] Milton BE, Keck JC. Laminar burning velocities in stoichiometric hydrogen and hydrogen-hydrocarbon gas mixtures. Combust Flame 1984;58(1):13–22.
[19] Yu G, Law CK, Wu CK. Laminar flame speeds of hydrocarbon+air mixtures with hydrogen addition. Combust Flame 1986;63(3):339–47.
[20] Ren JY, Qin W, Egolfopoulos FN, Tsotsis TT. Strain-rate effects on hydrogen-enhanced lean premixed combustion. Combust Flame 2001;124(4):717–20.
[21] Ren JY, Qin W, Egolfopoulos FN, Mak H, Tsotsis TT. methane reforming and its potential effect on the efficiency and pollutant emissions of lean methane–air combustion. Chem Eng Sci 2001;56(4):1541–9.
[22] Halter F, Chauveau C, Djebaïli-Chaumeix N, Gokalp I. Characterization of the effects of pressure and hydrogen concentration on laminar burning velocities of methane–hydrogen–air mixtures. Proc Combust Inst 2005;30(1):201–8.
[23] Di Sarli V, Di Benedetto A. Laminar burning velocity of hydrogen–methane/air premixed flames. Int J Hydrogen Energy 2007;32(5):637–46.
[24] Shen X, Xiu G, Wu S. Experimental study on the explosion characteristics of methane/air mixtures with hydrogen addition. Appl Therm Eng 2017;120:741–7.
[25] Dahoe AE, Zevenbergen JF, Lemkowitz SM, Scarlett B. Dust explosions in spherical vessels: the role of flame thickness in the validity of the 'cube-root law'. J Loss Prev Process Ind 1996;9(1):33–44.
[26] Dahoe AE. Laminar burning velocities of hydrogen–air mixtures from closed vessel gas explosions. J Loss Prev Process Ind 2005;18(3):152–66.
[27] Yan Y, Tang W, Zhang Li, Pan W, Yang Z, Chen Y, et al. Numerical simulation of the effect of hydrogen addition fraction on catalytic micro-combustion characteristics of methane-air. Int J Hydrogen Energy 2014;39(4):1864–73.
[28] Wang J, Huang Z, Tang C, Miao H, Wang X. Numerical study of the effect of hydrogen addition on methane–air mixtures combustion. Int J Hydrogen Energy 2009;34(2):1084–96.
[29] Hu G, Zhang S, Li QF, Pan XB, Liao SY, Wang HQ, et al. Experimental investigation on the effects of hydrogen addition on thermal characteristics of methane/air premixed flames. Fuel 2014;115:232–40.
[30] Li Y, Bi M, Li B, Zhou Y, Gao W. Effects of hydrogen and initial pressure on flame characteristics and explosion pressure of methane/hydrogen fuels. Fuel 2018;233:269–82.
[31] Ma Q, Zhang Q, Chen J, Huang Y, Shi Y. Effects of hydrogen on combustion characteristics of methane in air. Int J Hydrogen Energy 2014;39(21):11291–8.
[32] Wang T, Liang H, Lin J, Luo Z, Wen H, Cheng F, et al. The explosion thermal behavior of H_2/CH_4/air mixtures in a closed 20 L vessel. Int J Hydrogen Energy 2022;47(2):1390–400.
[33] Leyer JC. Contributions a l'étude des instabilités de la combustion et des phenomènes de transfer de chaleur aux parois dans le cas des combustions à volume constant. Rev Gén Therm 1970;98:121–38.
[34] Mitu M, Giurcan V, Razus D, Prodan M, Oancea D. Propagation indices of methane-air explosions in closed vessels. J Loss Prev Process Ind 2017;47:110–9.
[35] Wang LQ, Ma HH, Shen ZW. Explosion characteristics of hydrogen-air mixtures diluted with inert gases at sub-atmospheric pressures. Int J Hydrogen Energy 2019;44(40):22527–36.
[36] Zhang J, Zhou S, Su Y, Luo Z, Wang T. Experimental study of the influence of H_2/CO on the CH_4 explosion pressure and thermal behaviors. ACS Omega 2022;7(36):32432–41.
[37] Goldfarb I, Gol'dshtein V, Kuzmenko G, Sazhin S. Thermal radiation effect on thermal explosion in gas containing fuel droplets. Combust Theory Modell 1999;3(4):769–87.
[38] Lei B, Xiao J, Kuznetsov M, Jordan T. Effects of heat transfer mechanism on methane-air mixture explosion in 20 L spherical device. J Loss Prev Process Ind 2022;80:104864.
[39] Xiao J, Travis JR, Royl P, Necker G, Svishchev A, Jordan T. Three-dimensional all-speed CFD code for safety analysis of nuclear reactor containment: Status of GASFLOW parallelization, model development, validation and application. Nucl Eng Des 2016;301:290–310.
[40] Xiao J, Breitung W, Kuznetsov M, Zhang H, Travis JR, Redlinger R, et al. GASFLOW-MPI: a new 3-D parallel all-speed CFD code for turbulent dispersion and combustion simulations: Part I: Models, verification and validation. Int J Hydrogen Energy 2017;42(12):8346–68.
[41] Turns SR. An introduction to combustion, concepts and applications. New York: McGraw Hill; 1996.
[42] Xiao J, Travis JR, Kuznetsov M. Numerical investigations of heat losses to confinement structures from hydrogen-air turbulent flames in ENACCEF facility. Int J Hydrogen Energy 2015;40(38):13106–20.
[43] Rohsenow WM, Choi H. Heat, mass, and momentum transfer. Englewood Cliffs. New Jersey: Prentice-Hall; 1961.
[44] Li Y, Xiao J, Zhang H, Breitung W, Travis J, Kuznetsov M, et al. Numerical analysis of hydrogen release, dispersion and combustion in a tunnel with fuel cell vehicles using all-speed CFD code GASFLOW-MPI. Int J Hydrogen Energy 2021;46(23):12474–86.
[45] David WT. Radiation from flames. Nature 1942;150(3805):407–8.

[46] Hadjipanayis MA, Beyrau F, Lindstedt RP, Atkinson G, Cusco L. Thermal radiation from vapour cloud explosions. Process Saf Environ Protect 2015;94:517–27.
[47] Xiao J, Kuznetsov M, Travis JR. Experimental and numerical investigations of hydrogen jet fire in a vented compartment. Int J Hydrogen Energy 2018;43(21): 10167–84.
[48] Chandrasekhar S. Radiative transfer. New York: Dover Publications; 1960.
[49] Sparrow EM, Cess RD. Radiation heat transfer. Washington: Hemisphere Publishing; 1978.
[50] Sami M, Annamalai K, Wooldridge M. Co-firing of coal and biomass fuel blends. Prog Energy Combust Sci 2001;27(2):171–214.
[51] Di Blasi C. Modeling chemical and physical processes of wood and biomass pyrolysis. Prog Energy Combust Sci 2008;34(1):47–90.
[52] Jones WP, Lindstedt RP. Global reaction schemes for hydrocarbon combustion. Combust Flame 1988;73(3):233–49.
[53] Islas A, Fernandez AR, Betegon C, Martinez-Paneda E, Pandal A. Computational assessment of biomass dust explosions in the 20L sphere. Prog Energy Combust Sci 2022;165:791–814.
[54] Kim JP, Schnell U, Scheffknecht G. Comparison of different global reaction mechanisms for MILD combustion of natural gas. Combust Sci Technol 2008;180 (4):565–92.
[55] Zhang H, Li Y, Xiao J, Jordan T. Detached Eddy Simulation of hydrogen turbulent dispersion in nuclear containment compartment using GASFLOW-MPI. Int J Hydrogen Energy 2018;43(29):13659–75.